AIAA JOURNAL
Vol. 43, No. 7, July 2005

Flow Structure on Diamond and Lambda Planforms: Trailing-Edge Region

B. Yaniktepe* and D. Rockwell†
Lehigh University, Bethlehem, Pennsylvania 18015

The instantaneous and averaged flow structure on diamond and lambda planforms is characterized by using a technique of high-image-density particle image velocimetry. Emphasis is on the structure in the trailing-edge region, over a range of angle of attack. Elongated layers of vorticity in the crossflow plane exhibit well-defined mean (time-averaged) and instantaneous concentrations of vorticity. These features are interpreted in conjunction with patterns of streamline topology, as well as images of rms velocity fluctuation and velocity spectra obtained from space–time imaging.

Nomenclature

C	=	root chord of entire planform, mm
C'	=	root chord of leading (delta-wing) portion of planform, mm
f	=	frequency, Hz
S	=	local semispan of wing, mm
S_w	=	spectrum of w component of velocity fluctuation
U	=	freestream velocity, mm/s
V	=	magnitude of velocity vector, mm/s
v'	=	instantaneous velocity fluctuation in direction parallel to surface of wing, mm/s
w'	=	instantaneous velocity fluctuation normal to surface of wing, mm/s
w_{rms}	=	rms of velocity fluctuation, mm/s
x	=	distance from apex measured along plane of symmetry of wing, mm
y	=	distance measured normal to plane of symmetry of wing, mm
α	=	angle of attack, deg
Λ	=	sweep angle, deg
ψ	=	stream function, mm^2/s
ω	=	vorticity, 1/s
$\langle\,\rangle$	=	time-averaged value of quantity

I. Introduction

RECENT interest in unmanned combat air vehicles (UCAVs) has stimulated investigation of the flow structure on delta wings having low and moderate values of sweep angle, as well as on planforms that represent the actual UCAV configuration or simplifications thereof. Summaries of recent investigations, as well as unresolved issues, are given in the following.

A. Flow Structure on Delta Wings of Moderate and Low Sweep Angle

The distinctive features of the instantaneous and averaged flow structure on a delta wing of sweep angle $\Lambda = 50$ deg have been numerically computed by Gordnier and Visbal.[1] At low angle of attack, a dual primary vortex system is established, whereas at higher angle of attack, this dual structure gives way to a single, larger-scale vortex. Furthermore, the unsteadiness of the vortex core can involve a type of organized wandering at locations upstream of vortex breakdown. The form of vortex breakdown is more complex than for wings of relatively large sweep angle.

Honkan and Andreopoulos[2] determined patterns of instantaneous vorticity on a delta wing of sweep angle $\Lambda = 45$ deg via a pointwise technique and identified the existence of stationary discrete vortical structures, within the feeding sheet and the primary vortex. Furthermore, they determined the turbulence intensity in regions of shear-layer attachment and secondary separation. Miau et al.[3] investigated the flow patterns on a wing of sweep angle $\Lambda = 50$ deg, with a focus on the consequences of leading-edge profile. Ol and Gharib[4,5] undertook an experimental investigation of wings of $\Lambda = 50$ and 65 deg. They determined the onset of vortex breakdown by using dye visualization and, via a stereo particle-image-velocimetry (PIV) technique, defined various features of the leading-edge vortex structure, including a large-scale collapse of the rolled-up, leading-edge vortex. Taylor et al.[6] characterized the vortex flow patterns on a wing of low sweep angle, and in a further investigation, Taylor and Gursul[7] addressed the relationship between the vortex flow and buffeting of the wing surface. Yaniktepe and Rockwell[8] considered a wing of sweep angle $\Lambda = 38.7$ deg and focused on the flow structure well into the region of vortex breakdown including, at high angle of attack, the onset of a large-scale region of disordered flow structure beneath a highly organized vorticity layer.

B. Flow Structure on Highly Swept Wings

For wings of relatively large sweep angle, a single, large-scale vortex dominates the crossflow pattern. Well-defined vortical substructures can, however, occur about the periphery of this primary vortex. Visbal and Gordnier[9] summarize recent investigations of vortical substructures and describe their physical origin based on high-resolution numerical simulations. In addition, they assess three different interpretations of the substructures.

In recent decades, a range of experimental investigations has provided insight into the nature of these substructures. Early studies employed qualitative flow visualization to identify them, in unsteady and/or stationary forms. They include Squire et al.,[10] Gad-el-Hak and Blackwelder,[11,12] Payne et al.,[13] Lowson,[14] and Reynolds and Abtahi.[15] Further, time-averaged quantitative characterizations of vortical substructures involve the work of Verhaagen et al.,[16] Washburn and Visser,[17] Lowson et al.,[18] Riley and Lowson,[19] and Mitchell et al.[20]

The occurrence of vortical substructures was first computed by Gordnier and Visbal[21,22] who demonstrated their existence in the absence of external forcing. Mitchell et al.[23] and Mitchell and Molton[24]

Received 15 January 2004; revision received 10 January 2005; accepted for publication 17 January 2005.

*Visiting Research Scientist; currently Engineer, Sanayi ve Ticaret Bakanligi, No. 128-B, Maltepe, Ankara, Turkey.

†Professor, Department of Mechanical Engineering and Mechanics, 356 Packard Laboratory, 19 Memorial Drive West. Member AIAA.

also have computed patterns of vortical substructures using a different numerical approach.

C. Flow Structure on UCAV Planforms

Gursul et al.[25] summarized recent investigations of low-aspect-ratio wings and planforms and, furthermore, provide insight into the phenomena of vortex breakdown visualized by dye injection. The consequences of low sweep angle were clearly evident.

D. Unresolved Issues

The emphasis of the present investigation is on the unsteady flow structure, which serves as the origin of buffeting, with a focus on the configurations of diamond and lambda planforms. A central, generic feature of these planforms is an abrupt change in sweep angle of the leading edge, from a relatively low value to a value of 90 deg. The consequence of this sudden change on both the averaged flow structure and the flow unsteadiness has not been clarified. In particular, the following issues have not been addressed.

1. Crossflow Topology on Diamond and Lambda Planforms

The patterns of averaged streamline topology over crossflow planes on lambda and delta planforms are expected to be substantially different from those on a simple delta wing of low sweep angle. Basic definitions of topological features are defined by Perry and Steiner[26] and Chong et al.,[27] and in the following, certain of these features are described. The possibility of a well-defined focus (apparent center) of a tightly wound spiral pattern of streamlines, which might be located at the leading edge, rather than well inboard of it, would be an indication of the rapid flow distortion in the leading-edge region. In addition, the possibility of a saddle point, that is, an apparent intersection of streamlines, located outboard of the leading edge, has not been pursued in relation to the detailed geometry of the diamond and lambda planforms, including the geometry of the trailing edge.

Moreover, corresponding patterns of time-averaged vorticity, in relation to the streamline topology, have not been defined. It is expected, on the basis of investigations of a simple delta wing by Yaniktepe and Rockwell,[8] that an elongated layer of vorticity will form adjacent to the wing. The possibility, however, of a highly concentrated region of vorticity at the leading edge, which can be associated with the abrupt transformation of sweep angle, has not been addressed. Furthermore, the averaged patterns of vorticity can exhibit well-defined vortical substructures within the elongated layer from a diamond or lambda planform. For the case of a wing of relatively large sweep angle, where the flow pattern is dominated by a single large-scale vortex, the occurrence of such substructures is well established, as defined in the references given in the Introduction. The possibility that analogous, time-averaged vortical substructures can occur on wings with an abrupt change in sweep angle has not been pursued.

2. Instantaneous/Unsteady Flow Structure

The time-averaged features described in the foregoing are, of course, a consequence of the instantaneous flow structure. In particular, the instantaneous patterns of vorticity adjacent to the surface of the wing, in relation to possible time-averaged structures, have not been addressed for the wing planforms of interest herein. An important consequence of the instantaneous patterns of vorticity, as well as sequences of them, is the rms velocity fluctuation along the separated region adjacent to the surface of the wing. These patterns of rms velocity, along with the corresponding spectra, define the physical origin of unsteady (buffet) loading of the wing surface.

3. Objectives

The overall aim of the present investigation is to address the issues defined in the foregoing using a technique of high-image-density particle image velocimetry, which allows whole-field representations of both the time-averaged and instantaneous structure. Furthermore, a cinema mode of image acquisition allows, in effect, time records of the flow at a large number of locations, and thereby determination of the corresponding spectra of the fluctuating velocity field.

II. Experimental System and Techniques

Experiments were performed in a large-scale water channel, which had a test section 4928 mm long, 927 mm wide, and 610 mm high. This test section was preceded by a settling tank, a honeycomb-screen arrangement, and a 2:1 contraction. The turbulence intensity at the entrance to the test section was less than 0.3%.

The wings involved two basic planforms designated as diamond and lambda; they are shown in Figs. 1a and 1b. These figures show the system coordinates and critical length scales for each of the wings. The fore regions of the wings were matched. That is, the delta-wing portion of the leading region of each wing, having a

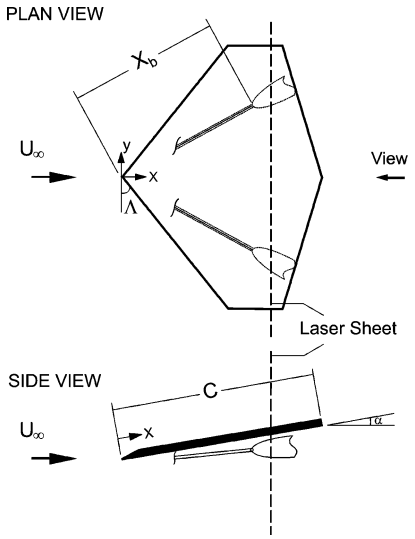

Fig. 1a Schematic of experimental system showing a representative wing, laser sheet location, and direction of view.

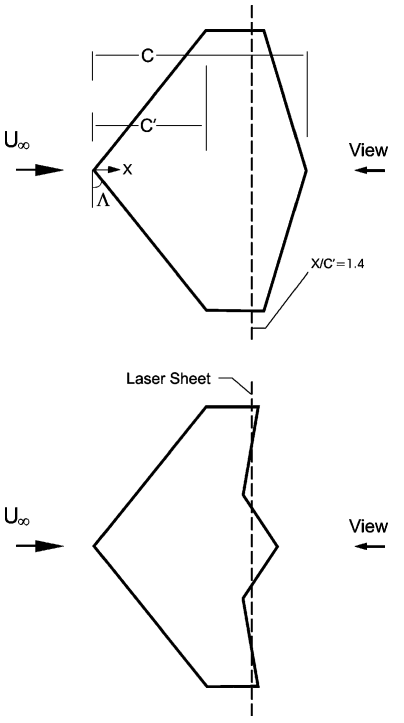

Fig. 1b Direct comparison of diamond and lambda planforms and locations of laser sheets employed for quantitative imaging.

chord $C' = 101.6$ mm, was maintained the same for each planform, in order to allow a direct comparison of the consequence of trailing-edge configuration on the flow development. The sweep angle of the leading edge of the wing was $\Lambda = 38.7$ deg. The chords C of the diamond and lambda wings had values, respectively, of 195 and 167 mm. This dimension C allows determination of all other dimensions of the wing via the schematics of Fig. 1b. In addition, each wing had a thickness t of 3 mm and was beveled on the windward side at an angle of 30 deg. The value of Reynolds number based on chord C was maintained at 10,000 for both wings. The corresponding values of freestream velocity for the diamond and lambda wings were $U_\infty = 51.4$ and 60.1 mm/s, respectively. The values of angle of attack were $\alpha = 7$, 13, 17, and 25 deg.

Emphasis is on global patterns of instantaneous flow structure and cinema sequences of these patterns, which allow characterization of the timewise evolution of the flow, as well as determination of the time-averaged structure. A technique of high-image-density PIV was employed. Illumination was provided by a dual-pulsed Yag laser system, having a maximum output of 90 mJ. The colinear beam from this dual system was transmitted through a system of cylindrical and spherical lenses, in order to generate a vertical laser sheet, which illuminated a desired crossflow plane, as indicated in Fig. 1a. The laser sheet was located at the trailing edge; in this region it is anticipated that the unsteady (buffet) loading will be severe. This location corresponds to the streamwise distance $x/C' = 1.4$, in which C' is the chord of the leading delta-wing configuration in each of the planforms, as designated in Fig. 1b. Based on preliminary dye visualization, it is estimated that the angle between the centerline of the predominant leading-edge vortex and the plane of the laser sheet is 60 deg. The flow is seeded with 12 micron-metallic-coated, hollow plastic spheres. Lack of significant buoyancy effects was ascertained by independent experiments, which indicated negligible downward or upward drift of particles within timescales an order of magnitude longer than the convective timescale C/U. In addition, a numerical simulation of particles in a simulated vortical flow showed insignificant radial particle drift for values of circulation characteristic of the present experiment. Patterns of these particle images were recorded on a high-resolution camera, having 1024 pixels $\times$ 1024 pixels. The effective framing rate of the camera was 15 cycles per second. This framing rate, relative to the characteristic frequencies of the major events of the flow structure, allowed a technique of cinema PIV for determination of spectra and cross spectra of the fluctuating flowfield.

The pattern of instantaneous velocity vectors was obtained by a cross-correlation technique involving successive frames of the patterns of particle images. Two sizes of interrogation windows were employed: 32×32 pixels and 16×16 pixels. In both cases, an effective overlap of 50% was employed, to satisfy the Nyquist criterion. The effective grid size for the larger interrogation window, in the plane of the laser sheet, was 2.65 mm. To ensure that the high-image-density criterion was satisfied, the number of particle images within the interrogation window was, at minimum, 15 to 20. The uncertainty of the velocity measurements was within 1.5%, and the uncertainty of vorticity was within 5.5%.

III. Dye Visualization of Flow Patterns

Representative patterns of the flow, visualized by dye injection, are shown in Fig. 2. At the lowest angle of attack $\alpha = 7$ deg, the dye was injected from two localized ports located at the apex of the wing. These ports were positioned to identify the locus of the vortex with the largest circulation formed from the leading edge. Substantial distortions of the dye marker are evident well upstream of the trailing edge of each wing; in an approximate sense this distortion sets in at about $x/C' = 1.0$, corresponding to the coordinates given in Fig. 1b. These distortions, or undulations, are highly nonstationary and are similar to the undulations prior to the onset of vortex breakdown calculated numerically by Gordnier and Visbal[1] on a delta wing of low sweep angle.

At the higher angle of attack $a = 13$ deg, the dye was injected along the windward side of the leading edge. The central portion of each wing is unmarked by dye, as it is continuously swept away by the streamwise velocity adjacent to the wing surface. On the other hand, exterior to this region, the dye is distributed over a large portion of the wing surface.

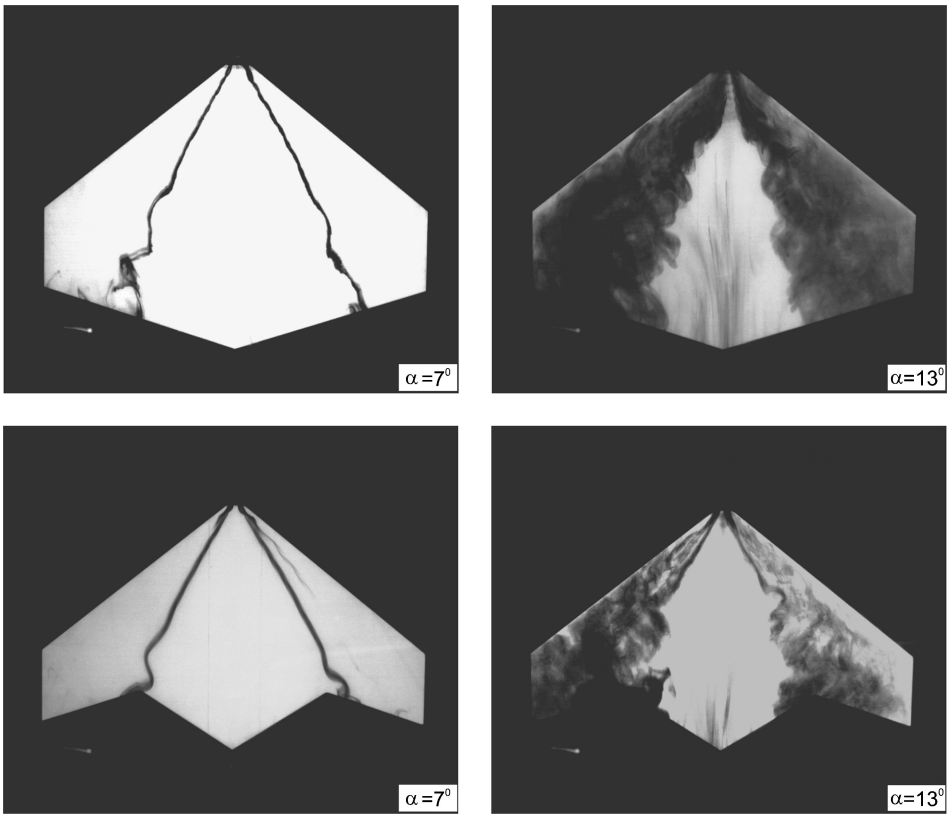

Fig. 2 Dye visualization at angles of attack $\alpha = 7$ and 13 deg. At $\alpha = 7$ deg, dye is injected from two localized ports at the apex of the wing, whereas at $\alpha = 13$ deg, it is injected along the leading edge on the windward side.

At higher angles of attack $a = 17$ and 25 deg considered in this investigation, the dye flooded the entire surface of the wing, and therefore these images are not shown.

IV. Patterns of Averaged Velocity and Streamline Topology

A. Velocity Patterns

Figure 3 shows patterns of averaged velocity $\langle V \rangle$ at angles of attack $\alpha = 7$, 13, 17, and 25 deg. The patterns for the diamond and lambda planforms are directly compared at each angle of attack. At $\alpha = 7$ deg, a common feature of the flow structure on both planforms is existence of a well-defined, small-scale swirl pattern at the leading edge. Furthermore, both wings exhibit relatively narrow, elongated patterns of velocity vectors, with a recirculation flow toward the leading edge of the wing. For the case of the lambda planform, the pattern is significantly distorted, apparently because of the gap occurring in the wing segment.

At $\alpha = 13$ deg, the intense, small-scale swirl pattern located at the leading edge, which was predominant at $\alpha = 7$ deg, no longer exists. For each wing, well-defined swirl patterns are evident, however, at the interface between the recirculating flow that returns to the leading-edge region and the flow exterior to this region. Furthermore, it is evident that the scale of the recirculation zone is smaller for the lambda planform.

At $\alpha = 17$ deg, small-scale swirl patterns are again evident at the interface between the elongated recirculation zone and the exterior flow. The predominant pattern for the lambda planform is closer to the leading edge than that for the diamond planform. This relative position of the swirl pattern is also evident at $\alpha = 13$ deg.

Finally, for the angle of attack $\alpha = 25$ deg, a well-defined, elongated swirl pattern no longer exists. Rather, flow is away from the wing surface toward the interface with the exterior flow. The overall spatial extent of this grossly separated flow pattern is approximately the same for both the diamond and lambda planforms.

B. Streamline Topology

Corresponding patterns of streamline topology, based on the averaged velocity patterns of Fig. 3, are shown in Fig. 4. At $\alpha = 7$ deg, for the diamond planform, the streamlines form a small-scale limit cycle immediately adjacent to the leading edge, whereas for the lambda planform, a localized swirl pattern occurs in this region. It is evident that the focus (apparent center) of both streamline patterns is located very close to the leading edge.

Furthermore, at $\alpha = 7$ deg, a saddle point, that is, the locus of an apparent intersection of streamlines, is located outboard of the leading edge of the diamond planform; no such saddle occurs for the diamond planform. These differences indicate that the trailing-edge configuration of the planform has a global influence on the streamline topology. A common feature of the streamline topology of both planforms, however, is the flow adjacent to the surface of the wing toward the leading edge; this return flow occurs over a relatively small width, in accord with the location of the interface of the corresponding patterns of averaged velocity $\langle V \rangle$ shown at $\alpha = 7$ deg in Fig. 3. Just inboard of the leading edge, this return flow merges with the small-scale swirl pattern at the leading edge to form a system of convergent streamlines known as a bifurcation line; it has not been observed previously in the cross-sectional topology of wings of either large or small sweep angle.

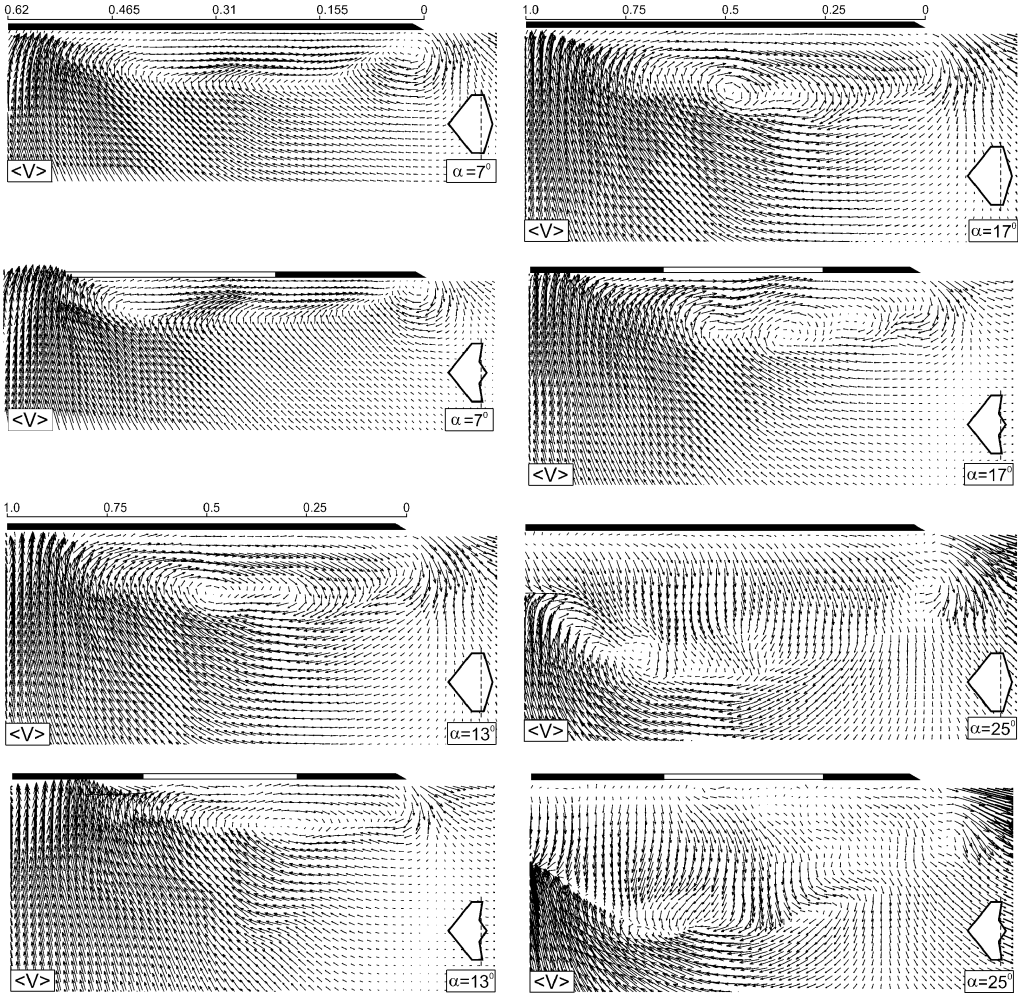

Fig. 3 Patterns of time-averaged velocity $\langle V \rangle$ at $\alpha = 7$, 13, 17, and 25 deg. For both the diamond and lambda planforms, the laser sheet is located at $x/C' = 1.4$, immediately downstream of abrupt change of sweep angle. The scale shown above the planform cross section is y/S, in which $y/S = 1.0$ corresponds to the plane of symmetry of wing; S is the semispan at $x/C' = 1.4$.

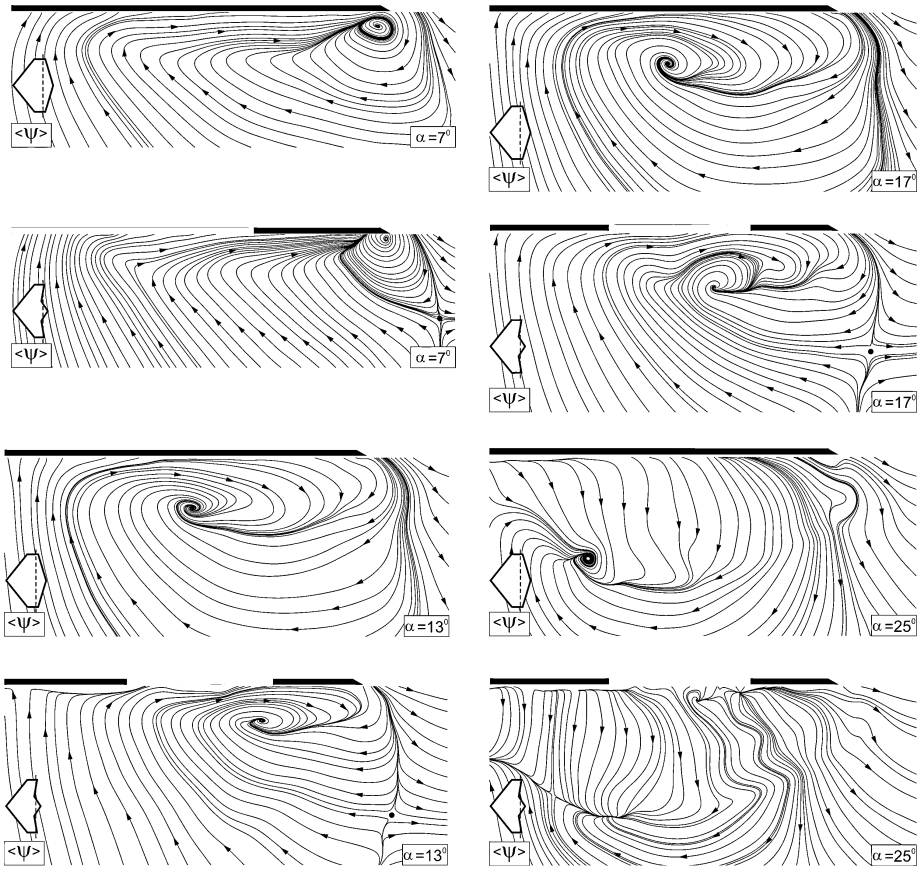

Fig. 4 Patterns of time-averaged streamline $\langle\Psi\rangle$ topology at angles of attack $\alpha = 7$, 13, 17, and 25 deg for the diamond and lambda planforms. For both planforms, the laser sheet is located at $x/C' = 1.4$, immediately downstream of abrupt change of sweep angle. The spanwise extent of each planform cross section is the same as in Fig. 3.

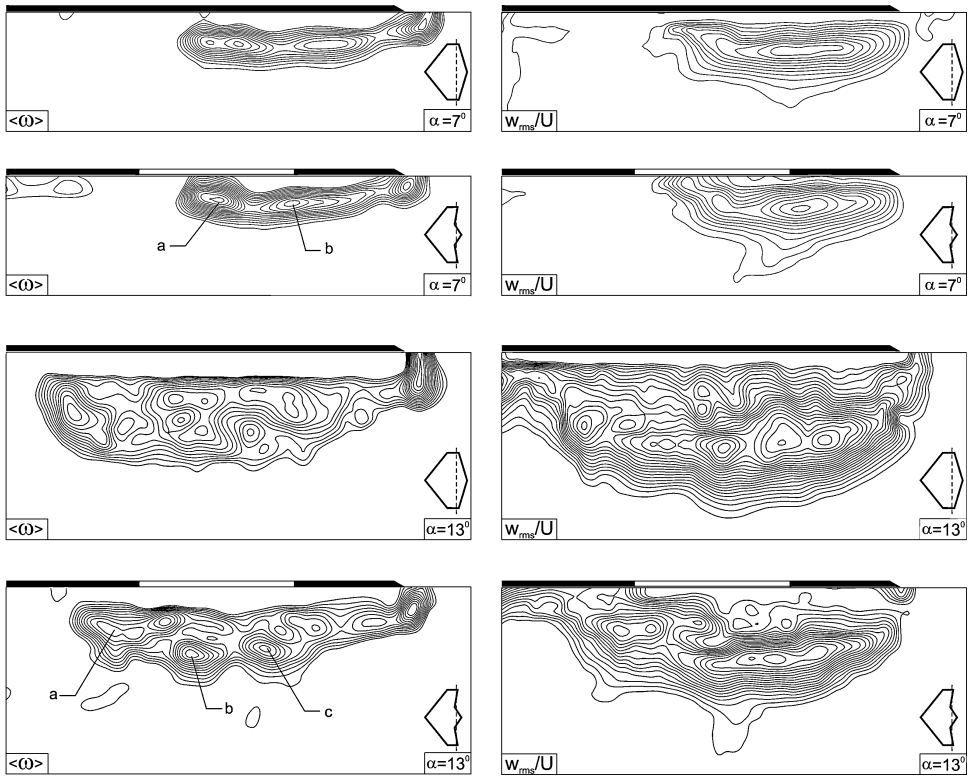

Fig. 5a Patterns of time-averaged vorticity $\langle\omega\rangle$ and corresponding patterns of rms velocity fluctuation w_{rms}/U (normal to the wing). At angle of attack $\alpha = 7$ deg, minimum and incremental values of vorticity contours are $[\langle\omega\rangle]_{min} = -0.2$ s^{-1}, and $\Delta[\langle\omega\rangle] = -0.15$ s^{-1}. At $\alpha = 13$ deg, $[\langle\omega\rangle]_{min} = -0.35$ s^{-1}, and $\Delta[\langle\omega\rangle] = -0.15$ s^{-1}. For patterns of rms velocity, minimum and incremental values at $\alpha = 7$ deg are $[w_{rms}/U]_{min} = 0.02$ and $\Delta\ [w_{rms}/U] = 0.01$. For $\alpha = 13$ deg, $[w_{rms}/U]_{min} = 0.04$ and $\Delta[w_{rms}/U] = 0.01$. For both the diamond and lambda planforms, the laser sheet is located at $x/C' = 1.4$, immediately downstream of abrupt change of sweep angle. In each image, the spanwise extent of the planform cross section corresponds to the semispan S of the wing at $x/C' = 1.4$.

At $\alpha = 13$ deg, foci are no longer evident at the leading edge of either planform, and the streamline topology reverts to a more classical form, which involves a single large-scale swirl inboard of the leading edge. For the lambda planform, the focus (apparent center) of this pattern is located closer to both the leading edge and the surface of the wing. Moreover, the saddle point evident at $\alpha = 7$ deg in the outboard region still persists at this angle of attack, although it is located further from the surface of the wing.

At $\alpha = 17$ deg, the overall characteristics of the patterns at $\alpha = 13$ deg are generally retained. On the other hand, at $\alpha = 25$ deg, the streamline patterns are indicative of a highly separated region adjacent to the surface of the wing, and it is not possible to identify a single, well-defined, large-scale swirl pattern.

The patterns of the averaged velocity $\langle V \rangle$ and streamline topology $\langle \Psi \rangle$ shown in Figs. 3 and 4 are associated with distinctive patterns of averaged vorticity $\langle \omega \rangle$ and velocity fluctuations w_{rms}/U, which are addressed in the next section.

V. Patterns of Averaged Vorticity and Fluctuating Velocity

The images of Figs. 5a and 5b show a direct comparison of the averaged vorticity $\langle \omega \rangle$ and rms velocity w_{rms}/U at angles of attack $\alpha = 7$, 13, 17, and 25 deg, for both the diamond and lambda planforms.

Consider the patterns of averaged vorticity $\langle \omega \rangle$ at $\alpha = 7$ deg in Fig. 5a. Both planforms exhibit a cluster of concentrated vorticity at the leading edge, which is associated with the localized swirl pattern of velocity shown at $\alpha = 7$ deg in Fig. 3 and the focus of the streamline topology at the leading edge at $\alpha = 7$ deg in Fig. 4. Furthermore, the patterns of vorticity are relatively elongated and contain two identifiable cells, or local concentrations of vorticity, designated as a and b, in addition to the vorticity concentrations appearing at the leading edge. These substructures are similar in form to those identified in the numerical simulation of Gordnier and Visbal[1] on a simple delta wing of low sweep angle. The corresponding patterns of transverse velocity fluctuation w_{rms}/U are generally similar for both planforms. The peak values are $[w_{\text{rms}}/U]_{\max} = 0.12$ and 0.13 for the diamond and lambda planforms, respectively.

At $\alpha = 13$ deg, the region of highly concentrated vorticity in the vicinity of the leading edge becomes even more pronounced, relative to that at $\alpha = 7$ deg, for both planforms. These concentrations at $\alpha = 13$ deg are, however, displaced further from the edge than those at $\alpha = 7$ deg. For this reason, they are not detectable in the corresponding streamline topology of Fig. 4. Furthermore, the vorticity layers appear as relatively elongated and have a substantially larger spanwise extent and width than at $\alpha = 7$ deg. Within these large-scale elongated layers, a number of smaller-scale concentrations

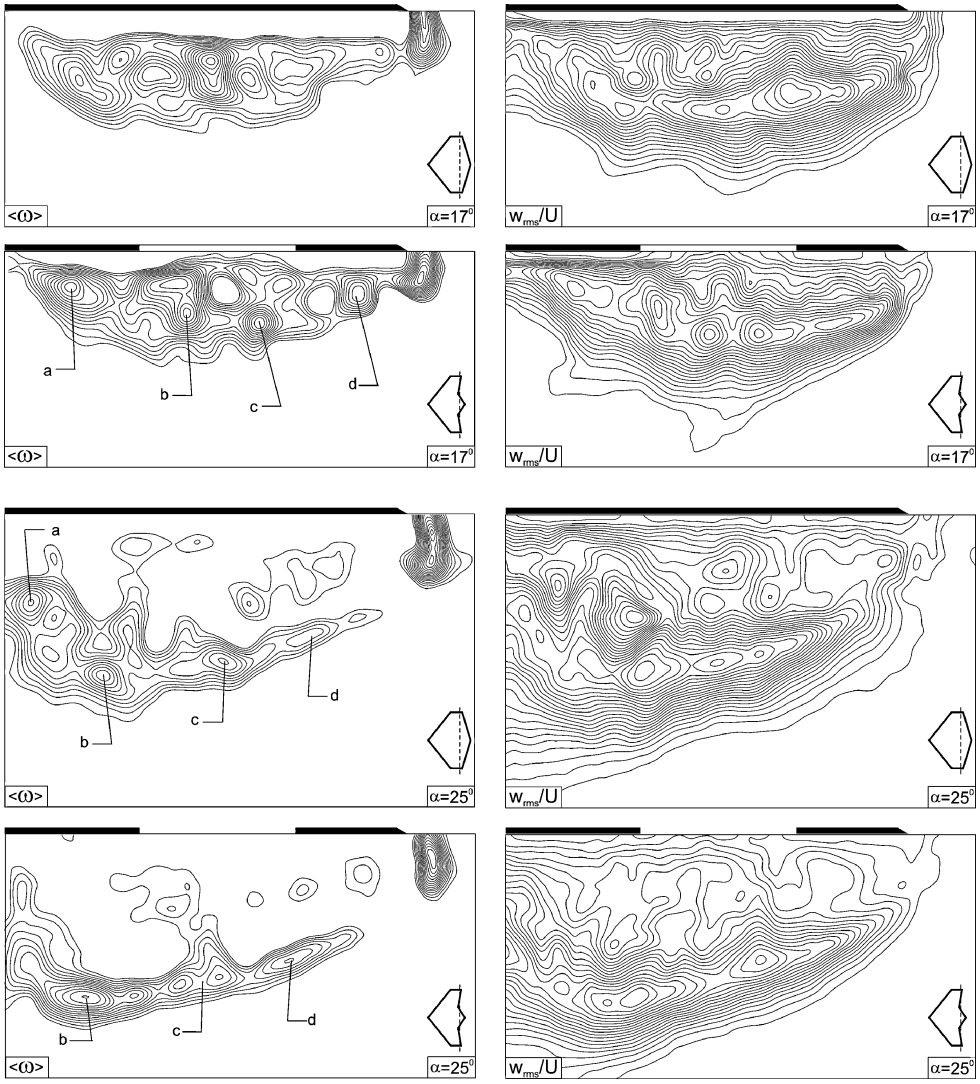

Fig. 5b Patterns of time-averaged vorticity $\langle \omega \rangle$ and corresponding patterns of rms velocity fluctuation w_{rms}/U (normal to the wing). At angle of attack $\alpha = 17$ deg, minimum and incremental values of vorticity contours are $[\langle \omega \rangle]_{\min} = -0.35\ \text{s}^{-1}$, and $\Delta[\langle \omega \rangle] = -0.15\ \text{s}^{-1}$. At $\alpha = 25$ deg, $[\langle \omega \rangle]_{\min} = -0.2\ \text{s}^{-1}$, and $\Delta[\langle \omega \rangle] = -0.15\ \text{s}^{-1}$. For contours of rms vertical velocity, at $\alpha = 17$ deg, $[w_{\text{rms}}/U]_{\min} = 0.03$, and $\Delta[w_{\text{rms}}/U] = 0.01$. For $\alpha = 25$ deg, $[w_{\text{rms}}/U]_{\min} = 0.02$, and $\Delta[w_{\text{rms}}/U] = 0.01$. For both the diamond and lambda planforms, the laser sheet is located at $x/C' = 1.4$, immediately downstream of abrupt change of sweep angle. In each image, the spanwise extent of the planform cross section corresponds to the semispan S of the wing at $x/C' = 1.4$.

of vorticity are evident at both $\alpha = 7$ and 13 deg. They are more clearly defined, however, for the lambda planform, and for purposes of simplicity in describing their existence individual structures are designated for this planform at $\alpha = 13$ and 17 deg. The predominant, distinctive concentrations at $\alpha = 13$ deg are indicated as a, b, and c. The corresponding patterns of rms velocity w_{rms}/U occupy a relatively large spatial extent, relative to the vorticity layer. Generally speaking, the maximum values of w_{rms}/U approximately correspond to the outer edge of the averaged patterns of vorticity $\langle\omega\rangle$. The peak value of velocity fluctuation is significantly high, that is, $[w_{\text{rms}}/U]_{\max} = 0.24$ and 0.20, respectively, for the diamond and lambda planforms.

Patterns corresponding to higher angles of attack $\alpha = 17$ and 25 deg are shown in Fig. 5b. At $\alpha = 17$ deg, the patterns of averaged vorticity $\langle\omega\rangle$ exhibit a generally similar, large-scale, elongated form as at $\alpha = 13$ deg. The pronounced concentration of vorticity adjacent to the leading edge persists for both planforms. Furthermore, identifiable concentrations of vorticity are evident in the large-scale, elongated layer. The most prominent are designated as a, b, c, and d on the lambda planform. The respective patterns of velocity fluctuation w_{rms}/U occupy a still larger spatial extent than at $\alpha = 13$ deg. The peak values are generally at the same spatial position as at the outer region of each of the large-scale patterns of averaged vorticity $\langle\omega\rangle$. The peak values of the velocity fluctuation are $[w_{\text{rms}}/U]_{\max} = 0.24$ and 0.22, respectively, for the diamond and lambda planforms.

For the highest angle of attack $\alpha = 25$ deg, the patterns of averaged vorticity $\langle\omega\rangle$ take on a fundamentally different form. They are displaced a substantial distance from the surface of the wing and, moreover, contain identifiable concentrations of smaller-scale vorticity, specified as a, b, c, and d. The locations of these smaller-scale concentrations are generally coincident with the peak values of velocity fluctuation w_{rms}/U. The peak values are $[w_{\text{rms}}/U] = 0.24$ and 0.2, respectively, for the diamond and lambda planforms. It is apparent that the layers of vorticity shown in Fig. 5b are formed at the interface between the highly separated region and the exterior flow indicated in the patterns of averaged velocity $\langle V\rangle$ at $\alpha = 25$ deg in Fig. 3. That is, this layer of relatively high vorticity exists adjacent to a large-scale region of separated flow.

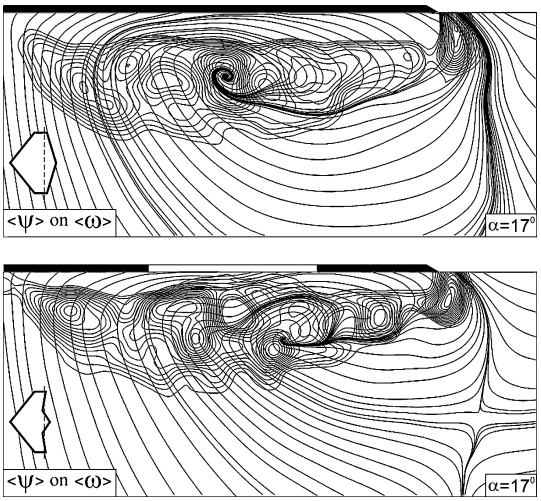

Fig. 6 Superposition of patterns of averaged vorticity $\langle\omega\rangle$ and streamline $\langle\Psi\rangle$ topology at $\alpha = 17$ deg for the diamond and lambda planforms. The laser sheet is located at $x/C' = 1.4$.

VI. Patterns of Averaged Vorticity and Streamline Topology: A Comparison

Certain patterns of averaged streamline topology shown in Fig. 4 suggest the existence of a single, large-scale leading-edge vortex, especially the patterns corresponding to the diamond planform at $\alpha = 13$ and 17 deg. This type of pattern, however, must be interpreted in conjunction with the corresponding pattern of averaged vorticity $\langle\omega\rangle$, as shown in Figs. 5a and 5b. The comparisons of Fig. 6 involve superposition of patterns of averaged vorticity $\langle\omega\rangle$ and averaged $\langle\Psi\rangle$ topology at $\alpha = 17$ deg for the diamond and lambda planforms. As emphasized earlier, the vorticity layer exhibits a narrow, elongated form, in contrast to the classical, nearly circular pattern of vorticity, which occurs on highly swept wings at sufficiently large angle of attack. For the diamond planform, the focus (apparent center) of the streamline pattern lies approximately midway along the elongated layer of vorticity. For the lambda planform, however, the focus is actually closer to the leading edge of the wing. In an overall sense, these streamline patterns do not indicate the presence of the well-defined, smaller-scale concentrations of vorticity.

The aforementioned coexistence of an elongated vorticity layer and a single spiral pattern of streamlines (with a single focus) appears to be an inherent feature of rapidly distorting flows separating

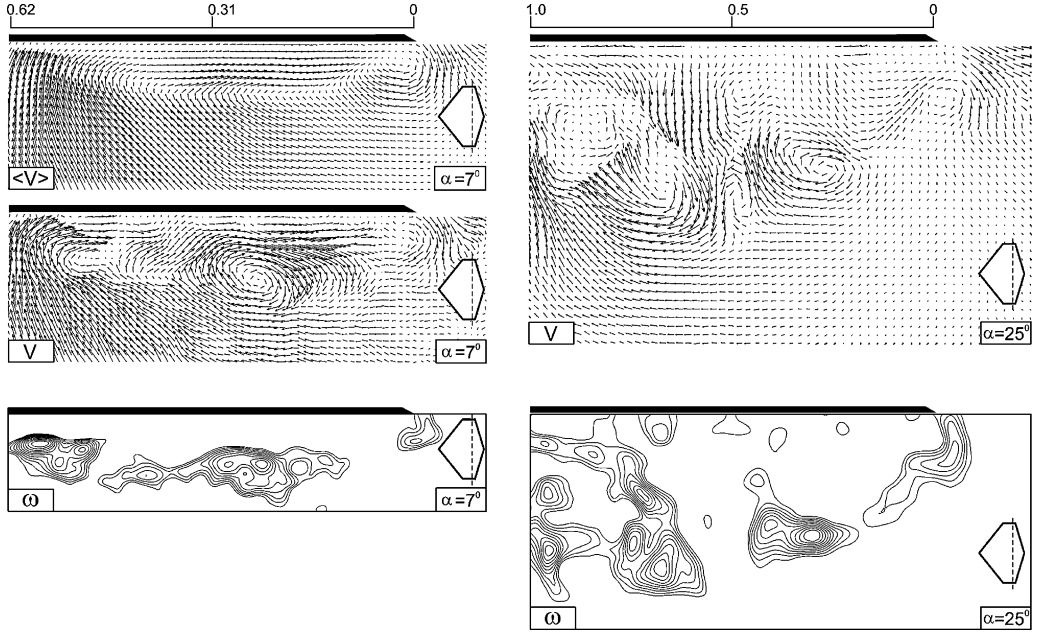

Fig. 7 Comparison of patterns of instantaneous velocity V and vorticity ω at angles of attack $\alpha = 7$ and 25 deg for the diamond planform. At $\alpha = 7$ deg, minimum and incremental values of vorticity are $\omega_{\min} = -1.5\ \text{s}^{-1}$, and $\Delta\omega = -0.5\ \text{s}^{-1}$. At $\alpha = 25$ deg, minimum and incremental values of vorticity are $\omega_{\min} = -0.5\ \text{s}^{-1}$, and $\Delta\omega = -0.5\ \text{s}^{-1}$. For both the diamond and lambda planforms, the laser sheet is located at $x/C' = 1.4$, immediately downstream of abrupt change of sweep angle. The spanwise extent of each planform cross section extends from $y/S = 0$ to 0.62 ($\alpha = 7$ deg) and to 1.0 ($\alpha = 25$ deg).

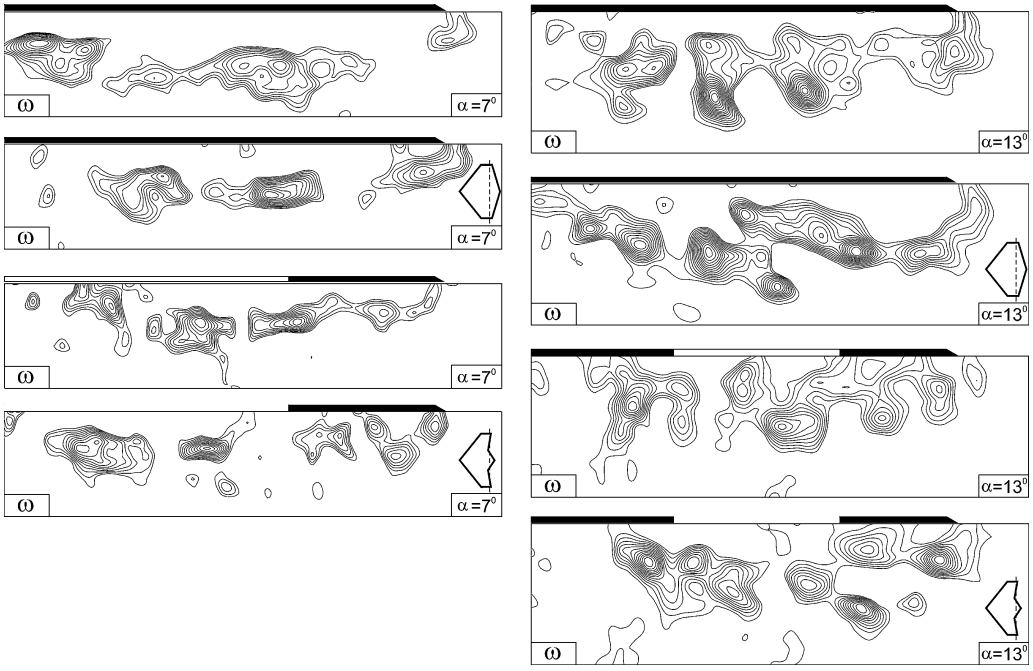

Fig. 8a Patterns of instantaneous vorticity ω at angles of attack $\alpha = 7$ and 13 deg for the diamond and lambda planforms. At $\alpha = 7$ deg, values of minimum and incremental levels of vorticity are $\omega_{min} = -1.5\ s^{-1}$, and $\Delta\omega = -0.5\ s^{-1}$. At $\alpha = 13$ deg, values of minimum and incremental levels of vorticity are $\omega_{min} = -0.5\ s^{-1}$ and $\Delta\omega = -0.5\ s^{-1}$. For both the diamond and lambda planforms, the laser sheet is located at $x/C' = 1.4$, immediately downstream of abrupt change of sweep angle. At $\alpha = 7$ deg (diamond and lambda planforms), the spanwise extent of the planform cross section extends from $y/S = 0$ (leading edge) to $y/S = 0.62$. For all other images, it extends from $y/S = 0$ to 1.0, where S is the semispan at $x/C' = 1.4$.

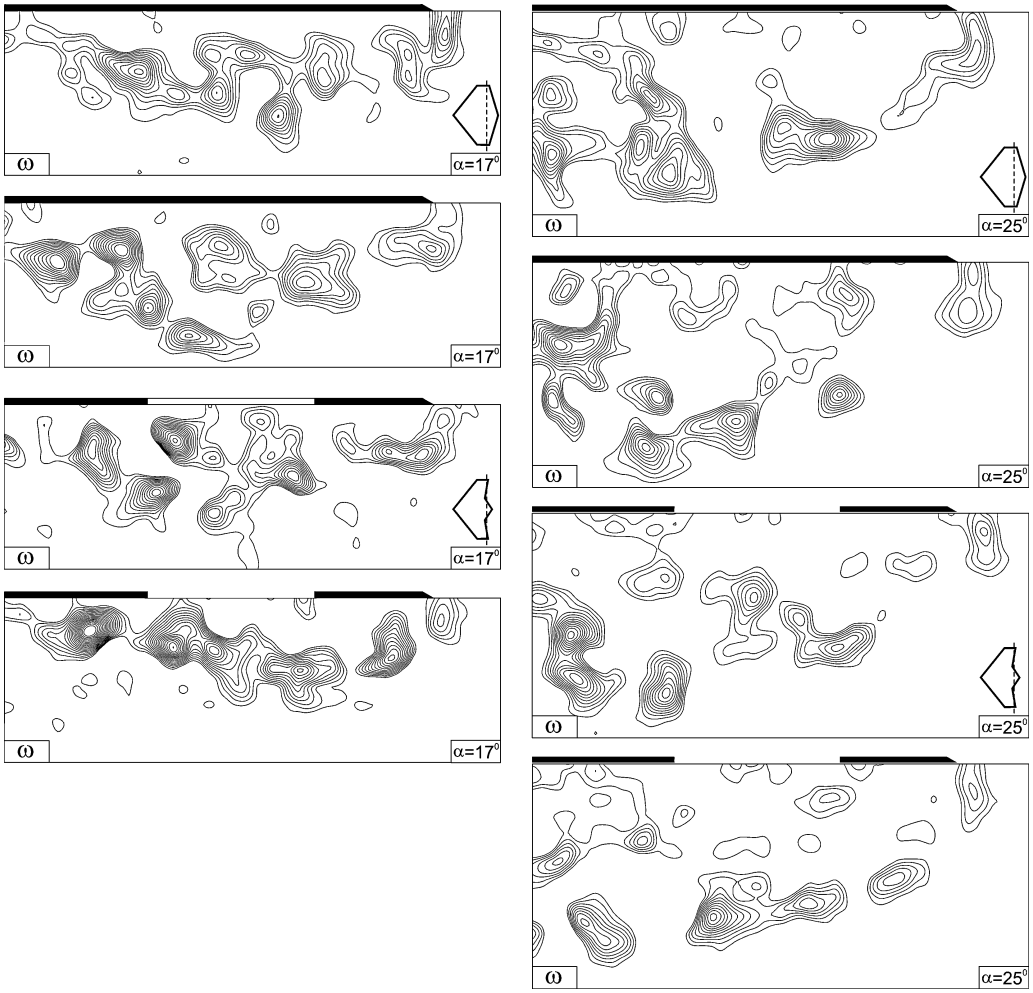

Fig. 8b Patterns of instantaneous vorticity ω at angles of attack $\alpha = 17$ and 25 deg for the diamond and lambda planforms. Values of minimum and incremental levels of vorticity are $\omega_{min} = -0.5\ s^{-1}$ and $\Delta\omega = -0.5\ s^{-1}$. For both the diamond and lambda planforms, the laser sheet is located at $x/C' = 1.4$, immediately downstream of abrupt change of sweep angle.

from a solid boundary. For the case of vortex formation in the very near wake of a cylinder, Akilli and Rockwell[28] observe conceptually similar patterns of streamline topology and vorticity layers. In this region of the wake, the boundary layer from the cylinder separates to form the elongated free shear layer.

Generally speaking, the existence of an elongated layer of vorticity in the crossflow plane from the leading edge of a delta wing has not been addressed for values of Reynolds number much higher than those employed herein. It is therefore an open issue as to whether the elongated structure described herein persists at high values of Reynolds number.

VII. Patterns of Instantaneous Vorticity

Patterns of instantaneous vorticity are shown relative to instantaneous velocity vectors in Fig. 7. In the left column, these patterns are compared at an angle of attack $\alpha = 7$ deg, along with the corresponding pattern of the averaged velocity $\langle V \rangle$, whereas in the right column they are compared for $\alpha = 25$ deg. Generally speaking, the identifiable clusters of vorticity are associated with well-defined swirls of patterns of velocity vectors.

To indicate the degree of variability of the instantaneous patterns of vorticity, Fig. 8a shows two images at each angle of attack α and for both the diamond and lambda planforms. Angles of attack $\alpha = 13$ and 17 deg are represented in Fig. 8a, while $\alpha = 17$ and 25 deg are shown in Fig. 8b. All patterns exhibit, from one instant to the next, significant variability in the precise location and level of the vorticity concentrations. Nevertheless, a quasi-ordered structure is apparent in each of the images, and, furthermore, it is possible to discern, in an approximate sense, the spacing between identifiable concentrations of vorticity. For each of the sets of instantaneous images, at each value of angle of attack α and each planform, the spacing between concentrations is, in most cases, roughly commensurate with the spacing between the time-averaged patterns of substructures a, b, c, and d shown in Figs. 5a and 5b. During the averaging process that yields the patterns of Figs. 5a and 5b, the instantaneous patterns of Figs. 8a and 8b are, in effect, smeared because of the variation in spatial position of the patterns of vorticity concentrations over the entire time sequence of instantaneous images. As a result, the peak values of vorticity and the patterns of Figs. 5a and 5b are typically much lower than the peak values in the corresponding instantaneous images.

VIII. Spectra of Fluctuating Velocity

The organized patterns of instantaneous vorticity shown in Figs. 8a and 8b are associated with definable spectral components of the velocity fluctuation w. These spectra $S_w(f)$ are shown in Fig. 9 for $\alpha = 7$ and 25 deg. Each spectrum is referenced to a specified location in the corresponding pattern of constant contours of rms velocity fluctuation $w_{\rm rms}/U$. At $\alpha = 7$ deg, for the diamond planform a well-defined spectral component emerges just inboard of the leading edge; its frequency is $f = 0.49$ Hz. (Dimensionless frequencies are given subsequently.) Farther along the separated layer, a higher-frequency component occurs; its value is $f = 1.49$ Hz, and it coexists with the aforementioned component at $f = 0.95$ Hz. For the lambda wing, organized spectral components are also detectable. They have values in the range $f = 0.77$–1.37 Hz.

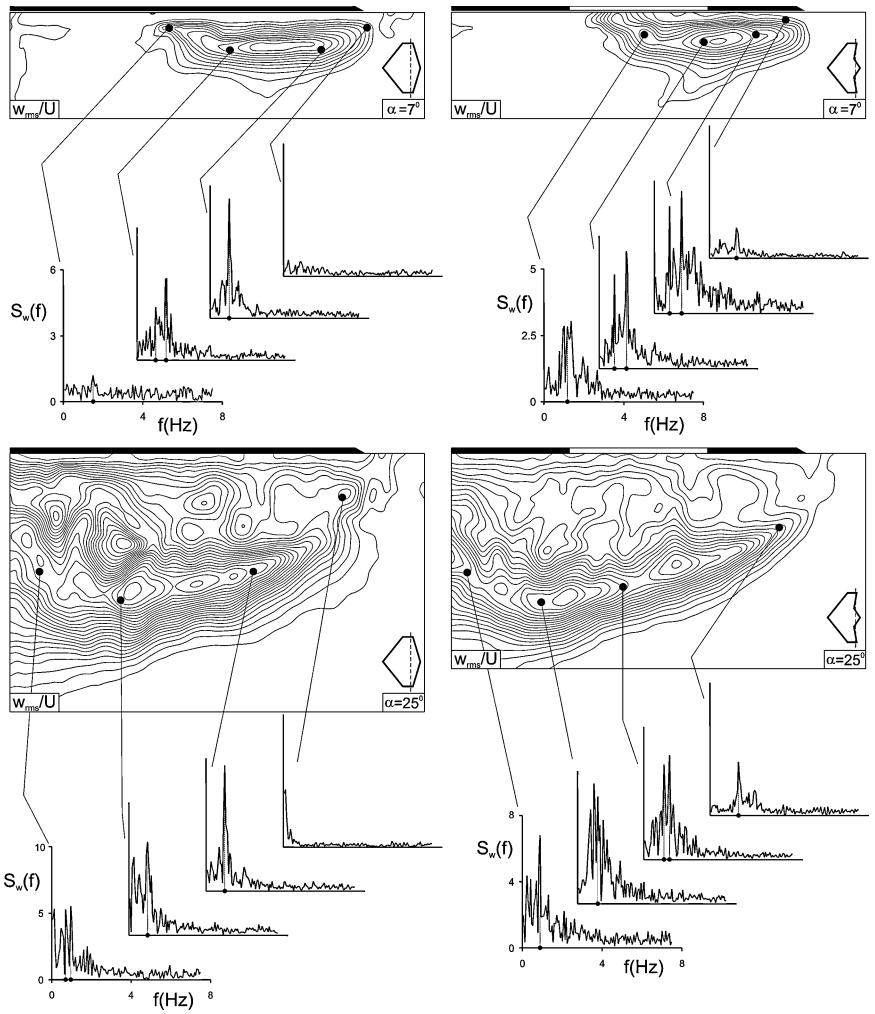

Fig. 9 Spectra $S_w(f)$ of the vertical velocity fluctuation w at locations corresponding to maxima of the rms value of the transverse (vertical) velocity fluctuation $w_{\rm rms}/U$ at angles of attack $\alpha = 7$ and 25 deg for the diamond and lambda planforms. The laser sheet is located at $x/C' = 1.4$.

As the vorticity layer tends to reattach to the surface of both lambda and diamond planforms the degree of organization, as well as the peak amplitude of the spectral component, both decrease. In fact, for the diamond planform the organized component is nearly entirely attenuated.

For the highest angle of attack, $\alpha = 25$ deg (diamond planform), an organized spectral component is clearly detectable at a significant distance from the leading edge. It has a value $f = 0.95$ Hz. This spectral component persists along the separated layer, and at the location farthest from the leading edge, components at $f = 0.71$ and 0.95 Hz are evident. For the lambda planform, at the location closest to the leading edge the spectral component is $f = 1.43$ Hz, and at locations further along the layer a single, well-defined component no longer occurs. Rather, the general peak is relatively broadband. The center frequencies of these rather broad distributions of peaks are indicated and have spectral components in the range $f = 0.83$–1.31 Hz.

For the diamond planform, the identifiable spectral peaks in Fig. 9 are in the range $0.71 \leq f \leq 0.95$ Hz, which corresponds to $2.69 \leq fC/U \leq 3.60$. For the lambda planform, the identifiable spectral peaks are in the range $0.77 \leq f \leq 1.43$ Hz, which corresponds to $2.13 \leq fC/U \leq 3.97$. For the case of a simple delta wing, Yaniktepe and Rockwell[8] found values of dimensionless frequency, based on spectral analysis, extending over the range of $0.51 \leq fC/U \leq 3.29$, and for a delta wing of sweep angle $\Lambda = 50$ deg, Gordnier and Visbal[1] computed a band of frequencies in the surface-pressure spectrum extending over the approximate range $1 \leq fC/U \leq 4.5$. Taken together, all of the foregoing results suggest that the organized unsteadiness associated with undulations or breakdown of the vortex core extend approximately over the range $0.5 \leq fC/U \leq 4.5$ for wings having a relatively low sweep angle. Remarkably, this range of frequencies approximates frequencies associated with the helical mode of instability of vortex breakdown of wings having relatively high sweep angle $1.0 \leq fC/U \leq 4$, as assessed by Menke et al.[29] and earlier works cited therein.

IX. Conclusions

The abrupt change in sweep angle, which is characteristic of both diamond and lambda planforms, along with the different trailing-edge configurations of these planforms, yields distinctive features of the patterns, relative to the case of a simple delta wing.

The streamline topology for both the diamond and lambda planforms shows, at low angle of attack, a focus (apparent center) of a spiral pattern of streamlines at the leading edge, rather than inboard of the leading edge. At moderate angle of attack, this focus shifts inboard of the leading edge, and at high angle attack, where a large-scale separated zone occurs adjacent to the wing surface, the pattern of streamline topology loses its ordered definition. Furthermore, the occurrence of saddle points (apparent intersection of streamlines) is influenced by a global effect of the trailing-edge configuration. For the lambda planform, a saddle point is located outboard of the leading edge; for the diamond planform, it is absent.

Corresponding patterns of vorticity show, at all values of angle of attack, a high concentration of vorticity in either the vicinity of, or even at, the leading edge. In the limiting case of low angle of attack, this concentration is nearly centered at the edge, whereas at larger angles of attack it is displaced significantly away from the edge. Furthermore, well-defined vortical substructures are identifiable in the elongated layers of time-averaged vorticity adjacent to the surface of the wing. These substructures appear to be analogous to those about the periphery of the single, large-scale region of vorticity on a wing of high sweep angle. Corresponding images of instantaneous vorticity show that the elongated layer of average vorticity is actually made up of well-defined vorticity concentrations, whose spacing is very approximately commensurate with those of time-averaged patterns. The spatial positions of these instantaneous vorticity concentrations exhibit substantial modulation from one instantaneous image to the next.

Contours of constant rms velocity fluctuation adjacent to the wing have extrema that are generally coincident with the outer regions of the elongated, time-averaged vorticity layers. The spectral content of these fluctuations, evaluated from space–time imaging, shows well-defined peaks, which are associated with the aforementioned modulation of instantaneous vorticity patterns. For extreme values of low and high angle of attack, the dimensionless frequencies of the spectral peaks lie in the range of $2.13 \leq fC/U \leq 3.97$.

Acknowledgments

The authors are grateful to the Air Force Office of Scientific Research (AFOSR), Grant F49620-02-1-0061, for support of this research program, which was monitored by John Schmisseur. The first author was supported jointly by AFOSR and Cukurova University during his research stay as a Visiting Scientist at Lehigh University. Prior to and subsequent to his stay at Lehigh, he has been supported as a Research Assistant at Cukurova University.

References

[1]Gordnier, R. E., and Visbal, M. R., "Higher-Order Compact-Difference Scheme Applied to the Simulation of the Low Sweep Delta Wing Flow," AIAA Paper 2003-0620, Jan. 2003.

[2]Honkan, A., and Andreopoulos, J., "Instantaneous Three-Dimensional Vorticity Measurements in Vortical Flow over a Delta Wing," *AIAA Journal*, Vol. 35, No. 10, 1997, pp. 1612–1620.

[3]Miau, J. J., Kuo, K. T., Liu, W H., Hsieh, S. J., Chou, J. H., and Lin, C. L., "Flow Developments Above 50-deg Sweep Delta Wings with Different Leading-Edge Profiles," *Journal of Aircraft*, Vol. 32, No. 4, 1995, pp. 787–794.

[4]Ol, M. V., and Gharib, M., "The Passage Towards Stall of Nonslender Delta Wings at Low Reynolds Number," AIAA Paper 2001-2843, June 2001.

[5]Ol, M. V., and Gharib, M., "Leading-Edge Vortex Structure of Nonslender Delta Wings at Low Reynolds Number," *AIAA Journal*, Vol. 41, No. 1, 2003, pp. 16–26.

[6]Taylor, G. S., Schnorbus, T., and Gursul, I., "An Investigation of Vortex Flows over Low Sweep Delta Wings," AIAA Paper 2003-4021, June 2003.

[7]Taylor, G., and Gursul, I., "Unsteady Vortex Flows and Buffeting of a Low Sweep Delta Wing," AIAA paper 2004-1066, Jan. 2004.

[8]Yaniktepe, B., and Rockwell, D., "Flow Structure on a Delta Wing of Low Sweep Angle," *AIAA Journal*, Vol. 42, No. 3, 2004, pp. 513–523.

[9]Visbal, M. R., and Gordnier, R. E., "On the Structure of the Shear Layer Emanating from a Swept Leading Edge at Angle of Attack," AIAA Paper 2003-4016, June 2003.

[10]Squire, B., II, Jones, J. G., and Stanbrook, A., "Investigation of the Characteristics of Some Plane and Cambered 65 Deg Delta Wings at Mach Numbers from 0.7 to 2.0," Aeronautical Research Council, R.M. No. 3305, 1963.

[11]Gad-el-Hak, M., and Blackwelder, R. F., "The Discrete Vortices from a Delta Wing," *AIAA Journal*, Vol. 23, No. 6, 1985, pp. 961–962.

[12]Gad-el-Hak, M., and Blackwelder, R. F., "Control of the Discrete Vortices from a Delta Wing," *AIAA Journal*, Vol. 25, No. 8, 1987, pp. 1042–1049.

[13]Payne, F. M., Ng, T. T., Nelson, R. C., and Schiff, L. B., "Visualization and Wake Surveys of Vortical Flow over Delta Wing," *AIAA Journal*, Vol. 26, No. 2, 1988, pp. 137–143.

[14]Lowson, M. V., "The Three-Dimensional Vortex Sheet Structure on Delta Wings," *Fluid Dynamics of Three-Dimensional Turbulent Shear Flows and Transition*, AGARD CP 438, Paper 11, 1988.

[15]Reynolds, G. A., and Abtahi, A. A., "Three-Dimensional Vortex Development, Breakdown and Control," AIAA Paper 89-0998, March 1989.

[16]Verhaagen, N. G., Meeder, J. P., and Verhelst, J. M., "Boundary Layer Effects on the Flow of a Leading Edge Vortex," AIAA Paper 93-3463, 1993.

[17]Washburn, A. E., and Visser, K. D., "Evolution of Vortical Structures in the Shear Layer of Delta Wings," AIAA Paper 94-2317, June 1994.

[18]Lowson, M. V., Riley, A. J., and Swales, C., "Flow Structure over Delta Wings," AIAA Paper 95-0586, Jan. 1995.

[19]Riley, A. J., and Lowson, M. V., "Development of a Three-Dimensional Free Shear Layer," *Journal of Fluid Mechanics*, Vol. 369, 1998, pp. 49–89.

[20]Mitchell, A., Molton, P., Barbaris, D., and Delery, J., "Vortical Substructures in the Shear Layers Forming Leading-Edge Vortices," AIAA Paper 2001-2424, June 2001.

[21]Gordnier, R. E., and Visbal, M. R., "Numerical Simulation of the Unsteady Vortex Structure over a Delta Wing," AIAA Paper 91-1811, June 1991.

[22]Gordnier, R. E., and Visbal, M. R., "Unsteady Vortex Structure over a Delta Wing," *Journal of Aircraft*, Vol. 31, No. 1, 1994, pp. 243–248.

[23]Mitchell, A., Morton, S., and Forsythe, J., "Analysis of Delta Wing Vortical Substructure Using Detached-Eddy Simulation," AIAA Paper 2002-2968, June 2002.

[24]Mitchell, A. M., and Molton, P., "Vortical Substructures in the Shear Layers Forming Leading-Edge Vortices," *AIAA Journal*, Vol. 40, No. 8, 2002, pp. 1689–1692.

[25]Gursul, I. Taylor, G., and Wooding, C. L., "Vortex Flows over Fixed-Wing Micro Air Vehicles," AIAA Paper 2002-0648, Jan. 2002.

[26]Perry, A. E., and Steiner, T. R., "Large-Scale Vortex Structures in Turbulent Wakes Behind Bluff Bodies. Part 1. Vortex Formation Processes," *Journal of Fluid Mechanics*, Vol. 174, 1987, pp. 233–270.

[27]Chong, M. S., Perry, A. E., and Cantwell, B. J., "A General Classification of Three-Dimensional Flow Fields," *Physics of Fluids A*, Vol. 2, No. 5, 1990, pp. 765–777.

[28]Akilli, H., and Rockwell, D., "Vortex Formation from a Cylinder in Shallow Water," *Physics of Fluids*, Vol. 14, No. 9, 2002, pp. 2957–2967.

[29]Menke, M., Yang, H., and Gursul, I., "Experiments on the Unsteady Nature of Vortex Breakdown over Delta Wings," *Experiments in Fluids*, Vol. 27, No. 3, 1999, pp. 262–272.

R. Lucht
Associate Editor